arTs Università degli Studi di Trieste
Archivio della ricerca – postprint

Dynamic and static identification of base-isolated bridges using Genetic Algorithms

Corrado Chisari *, Chiara Bedon, Claudio Amadio

Department of Engineering and Architecture, University of Trieste, Piazzale Europa, 1, 34127 Trieste, Italy

ARTICLE INFO

Accepted 27 July 2015

Keywords:
Dynamic and static identification
Genetic Algorithms
Numerical modelling
Bearing isolators
Bridges
Sensitivity analysis

ABSTRACT

In the paper, an identification approach based on a Genetic Algorithm (GA) is applied to the case study of a base-isolated, post-tensioned concrete bridge investigated in earlier contributions of literature. It is known that bearing isolators greatly influence the overall response of small- and medium-span bridges under dynamic loads, but in previous works it was seen that the characterisation of their elastic stiffness under small displacements may be inaccurate. In this work, based on in-situ test measurements obtained under static and dynamic loading conditions, inverse techniques based on GAs are successfully applied to the examined structural system, providing an efficient and well-calibrated structural identification of its main properties. Compared to other identification tools and classical correlation techniques, the main advantage deriving from the use of inverse approaches based on GAs typically manifests in the possibility to estimate a greater number of material parameters (e.g. properties of concrete as well as stiffness of the bearing isolators, etc.), and to critically assess the accuracy of the identification. Based on rather good correlation between test measurements and finite element (FE) model updating, it is expected that the same technique could be applied to various structural typologies and systems.

1. Introduction

The maintenance, safeguard and health monitoring of civil structures and bridges represent a topic of large interest for researchers, owners and users. Existing structures need to be assessed according the prescriptions of modern building codes; new constructions can benefit from the possibility of detecting any damage or loss of performance offered by continuous monitoring. In both cases, the analysis generally involves accurate numerical modelling of the structure, which must be calibrated according to the actual response (model updating) when it is excited by dynamic or static loads. A crucial step in the mechanical calibration of FE-models could derive, for example, from uncertainties on the actual boundary conditions, hence resulting in improper mechanical description of materials and inaccurate numerical investigations. This is the case of base-isolated structures, and specifically base-isolated bridges, where bearing-isolators are usually used to provide appropriate ultimate displacements under seismic events [1–5]. While the mechanical characterisation of these isolators under high-strain loads is typically provided by producers (e.g. [6]), however, it is well-known that "in-situ" static and dynamic tests carried out on bridge structures could induce in them maximum deformations markedly lower than their expected ultimate performances, hence resulting in difficult estimation and assessment of the effective in-plane horizontal stiffness provided by the isolation system. Structural identifications discussed in [7] for base-isolated bridges, for example, resulted in a satisfactory behaviour of the seismic isolators, but in identified bearing stiffnesses significantly higher than the reference experimental values. The lack of correlation between identified and experimental stiffness (and damping parameters) was justified in that case both by the application of low-strains only (e.g. magnified friction mechanisms and uncertainty in their estimation), and by the interference of non-structural components on the response of the whole structural systems or structural anomalies not taken into account during the design stage.

The calibration of material parameters and boundary conditions in numerical models can be performed by using the results from dynamic and static tests. The experimental modal analysis can be accomplished with three major testing procedures: ambient vibration [8], forced vibration [9] and free vibration [10]. A review of these three approaches may be found in [11]. Whichever testing procedure is used, some responses are measured and then used as input for the parameter calibration. Three basic types of data are used in dynamic identification: time domain, frequency domain

* Corresponding author. Tel.: +39 040 5583841.
E-mail addresses: corrado.chisari@gmail.com (C. Chisari), bedon@dicar.units.it (C. Bedon), amadio@univ.trieste.it (C. Amadio).

and modal model. During experimental modal analysis, the sampled time-series data are processed into the frequency response function (FRF) data. These frequency data are then further processed by curve fitting to obtain the modal model, namely the natural frequencies, damping ratios and mode shapes. Data from each of these steps may be used in the identification: see for example [12] (time-domain data), [13] (FRF data) and [14] (modal data). Static tests have comparatively less variety in the post-processing, since the measured responses are directly used in the calibration [15].

The identification process is carried out by inverting the forward operator, which links some parameters of the numerical model to the measured response. Since the explicit analytical inversion is not always possible, the solution is usually attained by solving an optimisation problem in which a discrepancy between experimental and computed data is minimised. In the literature, this approach is widely used in the field of deterministic inverse problems: differences exist in the formulation of the discrepancy (or cost) function to be minimised [16] and in the minimisation algorithm.

In this work, an approach for the characterisation of the main model parameters of an existing post-tensioned concrete, base-isolated bridge, based on the minimisation of a discrepancy function by means of a Genetic Algorithm (GA), is proposed. It makes use of the experimental data from the static tests and the dynamic properties (frequencies and modes) extracted via experimental modal analysis previously described in [17]. It is shown how different sources of information may be embedded within the same procedure for both dynamic and static identification. Unlike [17], where a simplified analytical procedure was proposed in order to estimate the stiffness of the isolators, here the set of unknown parameters is enlarged as to include Young modulus of the concrete constituting piers and deck, and the identifiability of all parameters is assessed by studying the relationship between the discrepancy function value and each parameter. Different formulations for the dynamic discrepancy function are proposed and critically discussed, and the differences in the results reasonably explained.

2. The identification process

Let us be given a physical system and a mathematical model describing it. The identification process consists of finding some parameters (constitutive parameters, boundary conditions, etc.) $\boldsymbol{p}$ of the mathematical model that give a "computed" response as close as possible to the experimental one. The "closeness" is made explicit by the definition of a discrepancy (or cost) function which measures the discrepancy between the two responses. Thus, the problem can be seen as an optimisation problem, in which the discrepancy function must be minimised in the process.

Some aspects are worth to be pointed out:

- The mathematical (numerical or analytical) model must be as representative as possible of the real behaviour of the structure. Any important feature affecting the response must be properly represented: anisotropy, nonlinear behaviour, boundary conditions, position and magnitude of masses, etc. A usual choice in engineering identification problems is to model the structure using a finite element (FE) discretization.
- The experimental setup must significantly involve the sought parameters, i.e. the sensitivity of the response to the variation of the parameters must be sufficiently high.
- All experimental data are affected by errors, and this must be accounted for in the definition of the response to be measured, in their post-processing (if needed) and in the accuracy of the results of the identification process.
- The analytical form of the discrepancy function $\omega(\boldsymbol{p})$ must take into account different precision of instrumentation when different types of measured variables are considered (loads, displacements, strains, frequencies, etc.). In the simplest form, it reads:

$$\omega(\boldsymbol{p}) = \boldsymbol{R}^T \boldsymbol{W} \boldsymbol{R} \tag{1}$$

  with $\boldsymbol{R} = \boldsymbol{y}^c(\boldsymbol{p}) - \boldsymbol{y}^m$ being the residual vector between some measured variables y_i^m, with $i = 1, \ldots, N$ (N number of measurements) and the computed counterparts y_i^c, that are obtained for a chosen set of trial parameters $\boldsymbol{p}$. $\boldsymbol{W}$ is a weight matrix that accounts for the correlation between response variables and the measurement scattering.
- Finally, the optimisation algorithm influences the accuracy of the results since, according the well-known "no free lunch theorem" [18], no algorithm is suitable for all problems. The presence of local optima, discontinuities in the function or in its derivatives can make the problem not solvable for some of them.

Each of these points will be exploited in this work. In particular, the optimisation algorithm is described in Section 3; the experimental setup and the FE model describing the structure are described in Sections 4.1 and 4.2, and a discussion about the sensitivity of the response on the sought parameters, the use of different discrepancy functions, the role of errors in the recorded data is presented together with the numerical application in Section 4.3.

3. The Genetic Algorithm

In order to solve the identification problem by minimising Eq. (1), a numerical iterative procedure must be used. To this aim, some of the most widely used approaches are gradient-based methods, such as Line Search [19] or Trust Region [20], which solve the problem by finding a stationary point of the discrepancy function. This strategy involves the computation of the Jacobian matrix of a solution candidate at each iteration and updating the point in the iterative process. Although computationally appealing, since the number of forward evaluations is generally rather low, these methods are local in scope, and can fail when the continuity and even the convexity of the cost function are not strictly satisfied in the search space. In this respect, global methods as Genetic Algorithms [21] are more general and they have been effectively employed in identification problems in previous research [22–25]. In addition to overcoming the mentioned drawbacks of gradient-based methods (by escaping local optima and not making use of derivatives), in this paper it will be shown that, in the GA framework, it is possible to qualitatively assess the identifiability of a parameter by studying the convergence process and the parameter–discrepancy function plots.

The main idea of this well-known approach is to let a *population* of several candidate solutions (*individuals*) evolve in the search of the optimum, throughout a certain number of *generations*. Compared to gradient-based algorithms, in which a single solution is updated in the search for the optimum, the use of populations of candidate solutions completely changes the perspective of the optimisation process. Clearly, the computational effort is usually higher in the GA approach, since one iteration consists of the evaluation of the discrepancy function for each individual in the population instead of a single candidate. On the other hand, the convergence may be seen as a process in which the population reduces its size in the parameter and fitness spaces, being distributed in the last generation around the best individuals [26]. The converged population distribution, thus, carries some information about the well-posedness of the problem, the number

of optima and the shape of the discrepancy function, allowing for considerations which are not possible using a gradient-based method. This will be shown in the following sections.

The first step of the procedure consists of the *chromosome* definition for the problem under study; it collects the parameters to be sought during the process. Each parameter x_i (called *gene*) is represented by a double-precision decimal varying between a lower and upper bound. The initial population can be generated randomly or with quasi-random techniques. In this work, a Sobol sequence [27] has been used, which allows for a more uniform exploration of the solution space than a simply random generation.

Processing a generation consists of evaluating the discrepancy value (*fitness* in the GA jargon) for each individual. After that, GA operators (selection, crossover and mutation) are applied to create a new generation of individuals. Selection is responsible of preparing the intermediate population for the crossover and mutation operators. Its basic function is choosing the parent couples; then, a new generation can be created through the application of crossover (or recombination) operator, with a probability p_c. In this work, the BLX-α Crossover [28] has been used. Furthermore, in order to improve convergence, an elitist approach has been applied [29], in which the best individual among parents and offspring is always placed (without undergoing the recombination operator) in the subsequent generation. Once the new population has been created, mutation is applied to some individuals according to a probability p_m, to prevent the loss of diversity of the population.

The process, schematically displayed in Fig. 1, continues with the evaluation of the created generation. From one generation to the next, the most promising genetic material spreads, the population fitness standard deviation decreases, and, if only one global optimum is found, also the parameter standard deviation decreases towards zero. Termination criteria are needed to end the process. In this work, the process has been stopped when a predefined number of generations has been processed.

The Genetic Algorithm has been implemented in ad-hoc software called TOSCA (Tool for Optimisation in Structural and Civil engineering Analyses) [30], successfully used in previous research for the estimation of model parameters for masonry structures [31].

4. A case study: The Dogna bridge

4.1. Description of the bridge and finite-element numerical modelling

A practical application of the aforementioned GA solving approach is proposed for a bridge recently investigated in [17,32]. The examined structural system, specifically, is located in the Municipality of Dogna (UD, Italy) a mountain area characterised by high level of seismic hazard and – based on the reference seismic design national standard [33] – a design peak of ground acceleration for a reference return period of 475 years equal to $a_g = 0.35$ g. The corresponding ground level is 'B', e.g. stiff soil, while the bridge is classified as strategic infrastructure.

The structure consists of a continuous, two-span post-tensioned reinforced concrete (RC) deck (C35/45 concrete, with $f_{ck} = 35$ MPa the cylindrical characteristic strength) with total length of 75 m, supported by a single mid-span elliptical, 4 m-width and about 10 m-height RC pier (C30/37 concrete, $f_{ck} = 30$ MPa) and two RC abutments (C30/37 concrete) able to provide lateral rigid supports at the deck ends.

The pier is supported by a fully rigid RC foundation block, namely consisting of a 2.5 m thick, hexagonal RC plate (8 m the

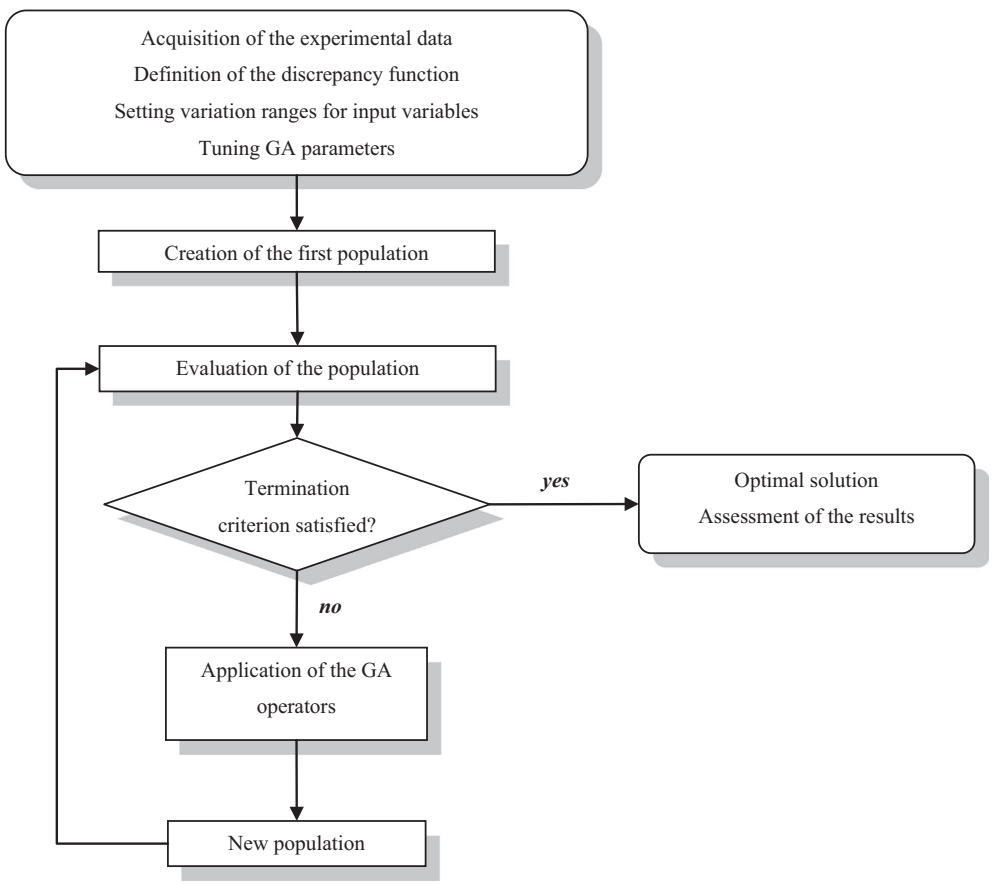

Fig. 1. Flow chart of the identification approach.

base dimension) supported by 18 m long RC bored piles (1.5 m the diameter of each one) and a stone ballast.

The transversal cross-section of the deck – characterised by a longitudinal 3% slope – is kept almost uniform along the bridge length, with the exception of the region near the central pier. An overview of the bridge is provided in Fig. 2, in the form of plan view and typical cross sections. For further technical details the reader is referred to [17,32].

The main characteristic of this bridge is given by the presence of six multi-directional cylindrical elastomeric bearing isolators – two for each support on pier and abutments – currently produced by FIP Industriale (type SI-N-1200/112 [6]).

These elastomeric isolators, having nominal diameter $\phi_{isolator}$ = 1200 mm and total thickness $h_{isolator}$ = 112 mm, consist of a series of steel laminates and hot-vulcanized rubber layers. Their main characteristics are given by large vertical stiffness (K_z = 7631 MN/m), as well as by high flexibility and damping capabilities under shear loads, hence resulting in nominal dynamic shear modulus G_{din} = 0.8 MPa, equivalent viscous damping coefficient ξ = 10–15%, and maximum allowable lateral displacement $u_{max} \approx 200$ mm [6]. The choice of this specific typology of elastomeric isolators was suggested, at the time of the bridge design, by the reference peak ground acceleration for the Dogna area. Despite their structural capabilities under extreme events such as high-level seismic events, however, the effective mechanical characterisation of these devices is rather complex to properly estimate at low strains [17].

In order to numerically investigate the Dogna bridge, a simplified but computationally efficient and accurate finite element (FE) model was carried out by means of the ABAQUS/Standard software package [34]. In it, careful consideration was devoted to the geometrical description of the bridge components, as well as their reciprocal interaction. At the same time, the use of a geometrically refined, full 3D solid FE-model was avoided, since inevitably associated to extremely onerous optimisation procedures.

In these hypotheses, the typical model consisted of 4-node, quadrilateral, stress/displacement shell elements (S4R) with reduced integration and large-strain formulation. A regular mesh pattern, composed of 0.5 m long × 0.25 m wide rectangular elements, was used for both the deck and the pier. In accordance with the available technical drawings, the pier was described by means of shell elements with middle plane lying in the (x, y) plane (see Fig. 3) and total thickness comprised between 0.95 and 2.4 m. At the same time, the typical transversal cross-section of the deck was described by means of shell elements lying on three separate planes (Fig. 3). In this manner, the effective transversal geometry as well as the longitudinal slope of the deck along its total span (3%) was properly accounted for. For the same reason, shell elements with variable thickness through the width and length of the deck (minimum 0.2 m, maximum 1.1 m) were then accordingly defined.

All the shell elements representative of the central portion of the deck were connected to the adjacent external portions by mean of "*tie*" rigid connectors able to provide a full rigid interaction between the interested nodes. Post-tensioning effects were neglected, since insignificant for dynamic identification purposes.

Material density for concrete elements was set equal to 2500 kg/m^3. At the same time, lumped masses were properly distributed along the bridge, in order to rationally take into account the inertial effects of footways (Fig. 3).

Concerning the mechanical characterisation of concrete, an isotropic, indefinitely linear elastic material was taken into account, with ρ_c = 2500 kg/m^3 the density, ν_c = 0.2 the Poisson' coefficient. Different nominal Young's modula E_c were assigned to the pier and to the deck respectively, and their values were assumed as two of the unknowns in the identification problems (see Section 4.3)

Careful consideration was finally given to the mechanical description of the seismic bearing devices. The structural interaction between the deck and the pier was guaranteed, specifically,

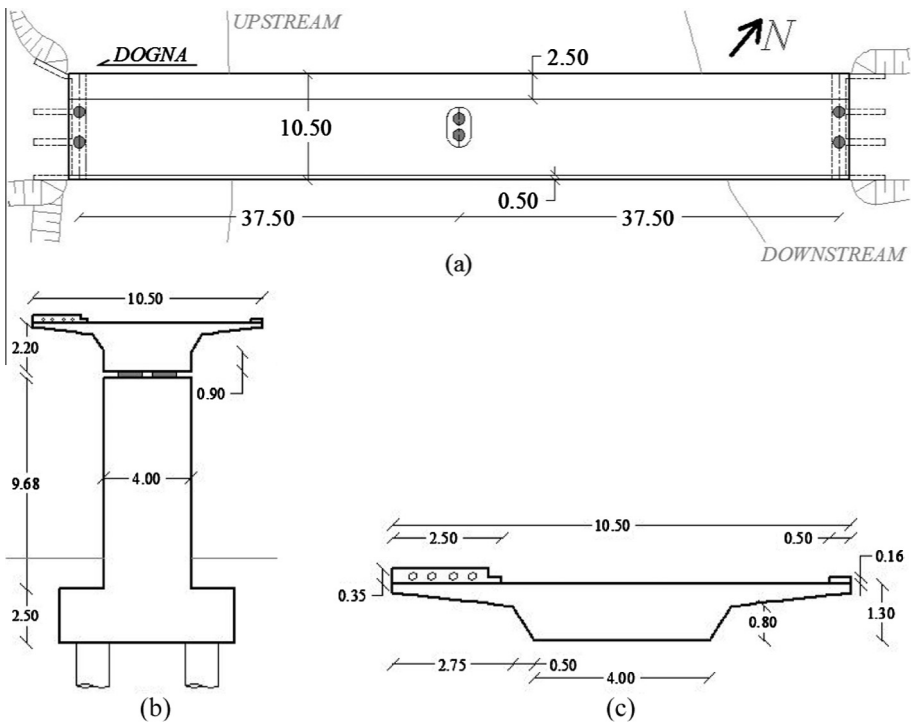

Fig. 2. Dogna bridge: (a) plan; (b) cross-section on the pier and (c) typical deck cross-section. Dimensions in meters.

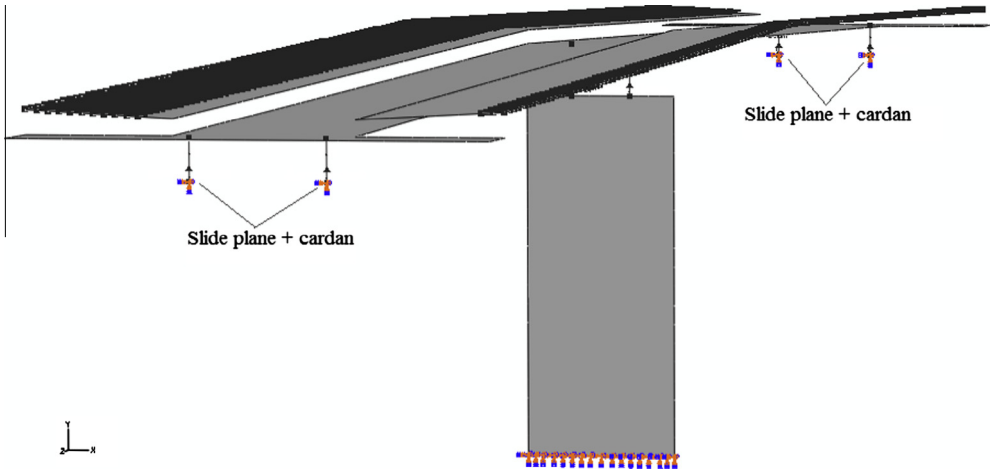

Fig. 3. Schematic view of the ABAQUS FE-model, axonometric view. In evidence, the lumped masses and the "*slide plane + cardan*" connectors representative of the elastomeric isolators.

by representing the elastomeric isolators in the form of assembled translational (*slide plane*) and rotational (*cardan*) connectors available in the ABAQUS library. *Cardan* connectors were used to take into account the rotational stiffness K_φ offered by the elastomeric isolators. Their rotational stiffness K_φ was estimated as $K_\varphi = (\pi\ R^4/4)\ K_z$, with $R = 0.6$ m the radius of the circular basis of the actual isolators and $K_z = 7631$ MN/m their nominal vertical stiffness [6]. At the same time, *slide plane* connectors able to provide infinitely rigid vertical stiffness K_z, and specific translational stiffnesses in the longitudinal and transversal directions K_y, K_x respectively were used. The same modelling approach was used both for the isolators on the pier and on the abutments.

The so assembled numerical model was used both for the dynamic and the static identification. In the first case, linear modal analyses were performed on a wide series of models having various mechanical properties, as discussed in Section 4.3. In the case of the static identification process, based on past static experiments performed on the studied bridge (Section 4.2.2), static incremental simulations were performed in ABAQUS/Standard.

4.2. Description of past experimental methods and results

Both dynamic and static experiments were performed on the mentioned bridge. Detailed discussion about methods and results of these past tests is provided in [17,32], while in this work only part of these experimental data will be taken into account for identification purposes.

4.2.1. Dynamic experiments

Harmonic, forced-vibration tests with low levels of excitation were performed, and steady-state harmonic vibrations were induced on the bridge by means of the stepped-sine technique. The exciter was mounted on the bridge deck approximately at one third of the span of the Dogna side, near the downstream sidewalk (Fig. 4). Dynamic investigations were carried out by the application of forces with maximum amplitude up to 19.5 kN. The range of exciting frequency comprised between 1 Hz and 15 Hz was examined and three separate dynamic experiments were performed, in order to excite the bridge along the transversal (T), longitudinal (L), and vertical (V) directions.

In all these tests, the dynamic structural response of the bridge was simultaneously measured by eighteen seismic accelerometers ICP (Series 393B12). Data sampling rate during testing was set equal to 0.05 Hz. For few cases only, a smaller step of 0.02 Hz

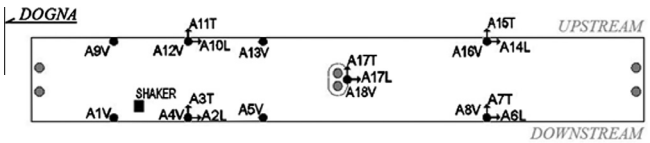

Fig. 4. Instrumental layout for the dynamic experiments. Position of the accelerometers for the measurement of the deck deformations along the vertical (V), transversal (T) and longitudinal (L) directions.

was used, to improve the detection of higher modes. The applied excitation forces generally resulted in maximum displacements of the bridge deck in the order of few millimetres.

The main dynamic parameters of the bridge – e.g. frequencies, damping ratios and related mode shapes – were then estimated by means of Experimental Modal Analysis (EMA) techniques based on multiple curve-fitting. Dynamic experiments and interpretation of measurements manifested in vibration modes with well separated resonance frequencies, with the exception of few modes only (modes (2, 3) and (6, 7)). The 12 identified vibration modes are listed in Table 1 [17].

4.2.2. Static experiments

Further static experiments were successively performed on the same bridge [17] by means of static truck-loads applied to the deck. Three different loading configurations, e.g. one torsional static scheme and two flexural schemes were considered. During the

Table 1
Experimental modal analysis results: mean value of natural frequencies p_r, with their maximum deviations. T = Torsional; B = Bending; RB = (almost) rigid-body motion [17].

Mode order r	Description	Natural frequency p_r (Hz)
1	1st B	2.022 ± 0.001
2	RB Transversal	3.053 ± 0.003
3	2nd B	3.180 ± 0.002
4	RB Longitudinal	3.605 ± 0.002
5	RB Torsional	4.831 ± 0.011
6	3rd B	6.887 ± 0.046
7	1st T	6.934 ± 0.015
8	2nd T	7.995 ± 0.005
9	4th B	9.107 ± 0.020
10	Coupled B-T	12.910 ± 0.025
11	Coupled B-T	14.228 ± 0.081
12	Coupled B-T	14.433 ± 0.100

experiments, vertical displacements of the deck were measured at 17 different locations (Fig. 5), (i) immediately after the application of the truck loads, (ii) after half an hour of loading and (iii) after the complete unloading of the bridge. As stated in [17], almost negligible discrepancies were generally found between the vertical deflections monitored at conditions (i) and (ii). In addition, the unloading of the bridge (iii) typically manifested null residual deformations.

4.3. The parameter identification

4.3.1. Introduction

In the following subsections, the inverse approach for the identification of the main material properties for the model previously described is applied. Three analyses are described:

1. Dynamic analysis 1 (D1): Dynamic identification based on the fundamental periods.
2. Dynamic analysis 2 (D2): Dynamic identification based on fundamental periods and modal shapes.
3. Static identification (S).

The analyses differ for the discrepancy function utilised, that will be described in each paragraph. The sought parameters are the transversal (K_x) and longitudinal (K_y) stiffnesses of the isolators, the pier and deck Young modulus, respectively $E_{c,pier}$, $E_{c,deck}$. The variation range for each parameter is displayed in Table 2. Since high uncertainty exists for the isolator stiffnesses, they are allowed to vary largely in the optimisation process. The values declared by the manufacturer and those estimated in [17] are contained in the range. The variability of the Young modulus for pier and deck is minor, since the class of concrete is known in advance.

The choice of the parameters used in the GA is very problem-dependent. In general, some of the parameters control the exploration capabilities of the algorithm (population size, crossover parameters, mutation probability); others govern the evolution and thus the convergence (scaling pressure, number of generations). Tuning such parameters depends on the shape of the function to minimise and the computation budget available, since for non-trivial discrepancy functions as those proposed in this work each individual evaluation implies running a FE analysis. For the problem under study, it was found that the following parameters were a sufficient trade-off between exploration and convergence:

- Population size: 50 individuals.
- Number of Generations: 50.
- Crossover probability: 0.85.
- Mutation Probability: 0.02.
- Scaling pressure: 1.7.
- Parameter α for BLX: 2.0.

4.3.2. Dynamic identification based on fundamental periods (D1)

As described before, dynamic tests allow for the determination of the basic dynamic properties of the structures, basically modal shapes and periods. For the analysed bridge, the first identification

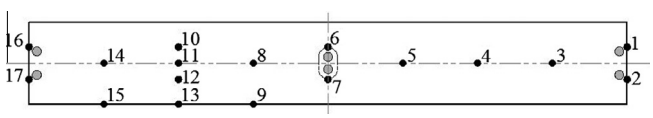

Fig. 5. Plan view of the instrumental layout for the static experiments. Position of control points for the measurements of the deck vertical deflections.

Table 2
Variation range of the sought parameters.

Parameter	Lower bound	Upper bound	Step
K_x (MN/m)	7.5	800	0.01
K_y (MN/m)	7.5	800	0.01
$E_{c,pier}$ (GPa)	20	60	1
$E_{c,deck}$ (GPa)	20	60	1

attempt was based on the discrepancy between the computed and measured periods. The cost function to be minimised is, thus:

$$\omega_{1,dyn}(\boldsymbol{p}) = \sum_{i=1}^{N_M} \left(\frac{T_{i,comp}(\boldsymbol{p}) - T_{i,exp}}{T_{exp,max}} \right)^2 \tag{2}$$

where $N_M = 12$ is the number of modes utilised; $T_{i,comp}(\boldsymbol{p})$ is the ith computed period; $T_{i,exp}$ is the ith experimental period and $\boldsymbol{p}$ is the vector of the sought parameters.

In Fig. 6 the mean and the best discrepancy value in the population are plotted against the generation number. It is possible to see that the mean value of the discrepancy becomes stable (despite some peaks due to mutated elements at some generations) at about generation 21, and it is clear that even in terms of best individuals the analysis finds the optimum at the same generation.

The material parameters identified so far (best individual) are shown in Table 3. Some comparisons may be done with the solution of the identification problem described in [17]. In the mentioned work, the authors set the concrete Young modulus to the value $E_{c,pier} = E_{c,deck} = 43.20$ GPa, which is in good agreement with the deck value found in the optimisation analysis. The isolator stiffnesses were obtained by means of an analytical formulation based on the comparison between the measured and computed frequencies for the fundamental rigid-body modes along longitudinal and transversal direction. The so found values were $K_x = 151.2$ MN/m and $K_y = 172.4$ MN/m, with difference with respect to the optimised values obtained in this study equal to about 18.7% and 0% respectively.

In this context, it should be noticed that the elastic stiffness of the used rubber bearing isolators is rather complex to correctly estimate. While experiments are generally performed by producers to certify the structural behaviour of seismic isolators under large lateral displacements, their basic mechanical properties under small displacements are often neglected, hence resulting in a possible improper calibration of numerical models. The nominal values of the stiffness supplied by the manufacturer for this class of isolators were $K_x = K_y = 89.7$ MN/m, about 50% less than the values estimated in this study.

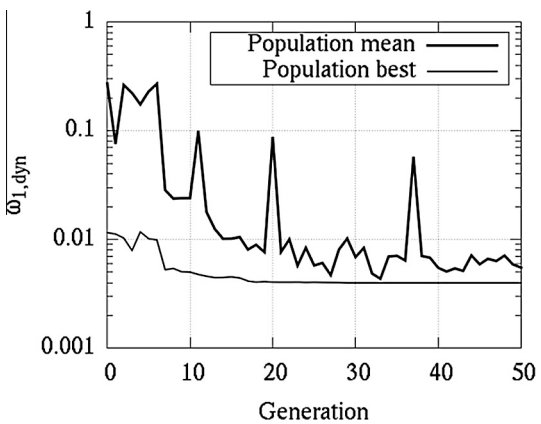

Fig. 6. Mean and best discrepancy value in the population against the generation number for dynamic analysis based on periods (D1).

Table 3
Solution of the analysis D1.

Parameter	Value
K_x (MN/m)	186
K_y (MN/m)	172.9
$E_{c,pier}$ (GPa)	39.1
$E_{c,deck}$ (GPa)	44.9

Table 4
Comparison between identified model frequencies and experimental outcomes of the first identification problem.

Mode number	Experimental period (s)	Numerical period (s)	Δ (s)	Δ (%)
1	0.495	0.496	0.002	0.39
2	0.328	0.332	0.005	1.48
3	0.314	0.310	−0.004	−1.29
4	0.277	0.277	0.000	−0.01
5	0.207	0.208	0.001	0.42
6	0.145	0.141	−0.004	−2.81
7	0.144	0.130	−0.014	−10.02
8	0.125	0.115	−0.010	−7.86
9	0.110	0.107	−0.003	−2.85
10	0.077	0.102	0.024	31.61
11	0.070	0.071	0.001	1.57
12	0.069	0.067	−0.002	−2.70

A comparison between the solution of the identification problem using Genetic Algorithm and the experimental data in terms of periods in displayed in Table 4, where the discrepancy between the periods is called Δ. It is clear than the discrepancies for the higher modes are larger in percentage, and it is an obvious consequence of the discrepancy function adopted. However, considering that experimental data for the higher modes are affected by a sensibly smaller accuracy, it may be considered acceptable.

It is common practice to use the Modal Assurance Criterion (MAC) [35] to determine the consistency between two modal shapes, i.e. a computed and a measured one. It is defined as:

$$MAC_{ij} = \frac{\left(\boldsymbol{\phi}_i^T \cdot \boldsymbol{\phi}_j\right)^2}{\boldsymbol{\phi}_i^2 \boldsymbol{\phi}_j^2} = cos^2\alpha \tag{3}$$

where $\boldsymbol{\phi}_i$ and $\boldsymbol{\phi}_j$ are the two modal vector to be compared, and α is the angle between them. This value is independent of the scaling adopted, that may be different between the computed modal shape and the experimental one; it assumes value equal to 1 in the case of perfect consistency (parallel vectors) and zero for orthogonal vectors.

Table 5 presents the MAC matrix of the experimental versus numerical modes, whose modal shapes are proposed in Fig. 7. It can be seen that the consistency between the modes is very high for the first five modes (MAC indices greater than 80%) and mode 9. Experimental modes 10, 11 and 12 do not have a numerical counterpart (all MAC indices are less than 30%), while some switches occur for modes in the range 6–8. In particular, experimental mode 6, 7, 8 are consistent respectively with numerical mode 8, 6 and 10.

It is interesting to see how the population parameters are distributed in their variation range when the minimum mean discrepancy in the population is approximately attained (as said, at generation 21). The results are displayed in the histograms of Fig. 8. It is immediately noticeable that while three parameters, namely K_x, K_y and $E_{c,deck}$ clearly converge towards a limited subset of the initial variation range, $E_{c,pier}$ is instead rather dispersed. It means that its influence on the overall discrepancy function is sensibly less important than the other parameters, and thus, its identification is less accurate.

It is confirmed by the parameter–discrepancy plot displayed in Fig. 9. Going towards the minimum values of discrepancy (ordinates), K_x, K_y and $E_{c,deck}$ (abscissa) converge towards the solution value. On the other hand, $E_{c,pier}$ remains undetermined, since the sensitivity of the discrepancy function to the variation of the parameter is quite small.

4.3.3. Dynamic identification based on fundamental periods and modal shapes (D2)

Some aspects of the identification analysis based on fundamental periods D1 may be pointed out:

1. Some switches between experimental and computed modal shapes sometimes occur. In the previous analysis a sequential mode pairing was used, in which the *i*th computed period was compared with the *i*th experimental period. Another possible choice is pairing periods corresponding to the same modal shape.
2. Based on the experimental response, uncertainty in the determination of the experimental periods is always present, and it is not the same for all modes.
3. No information about mode consistency was considered in the discrepancy function.
4. The higher modes, beyond the difficulty in the determination, have less influence in the global response when the structure is subjected to dynamic loads, because they are associated to smaller participating masses and modal amplitudes.

Because of all these considerations, a different discrepancy approach is proposed here, in which two objectives (period and modal shape discrepancy, respectively) are minimised. It is summarised by the following flow:

Table 5
MAC (%) matrix between experimental and numerical modes for the first identification problem.

Experimental modes	Numerical modes											
	1	2	3	4	5	6	7	8	9	10	11	12
1	99.04	0.02	8.13	0.41	0.00	0.27	0.00	0.01	0.01	0.07	0.01	13.31
2	0.00	83.47	0.19	0.00	5.88	0.00	11.81	0.79	0.03	0.05	0.87	0.00
3	21.77	0.16	88.62	0.08	0.00	0.04	0.02	0.02	11.86	0.05	0.00	9.96
4	0.21	0.00	0.00	99.20	0.03	1.15	0.00	0.00	0.00	0.00	0.01	0.14
5	0.00	3.89	0.01	0.01	94.08	0.00	0.70	0.06	0.01	0.00	15.65	0.01
6	3.54	2.97	0.34	0.04	0.02	1.13	17.54	83.40	7.52	6.48	0.28	0.01
7	0.12	0.01	5.80	0.40	0.00	96.05	0.05	0.62	56.07	0.00	0.00	0.05
8	2.08	0.72	0.06	0.01	0.23	0.01	4.58	23.24	3.10	89.94	1.62	0.20
9	0.46	0.07	8.26	0.24	0.00	50.29	0.80	2.74	88.54	0.87	0.02	4.41
10	0.26	0.38	21.84	0.05	0.00	17.24	1.75	15.96	10.31	0.02	0.19	0.15
11	0.66	0.09	1.30	0.09	0.01	15.79	0.18	0.01	28.31	7.49	0.06	11.94
12	8.08	0.08	0.07	0.00	0.07	7.26	0.35	0.40	4.06	25.81	0.83	19.36

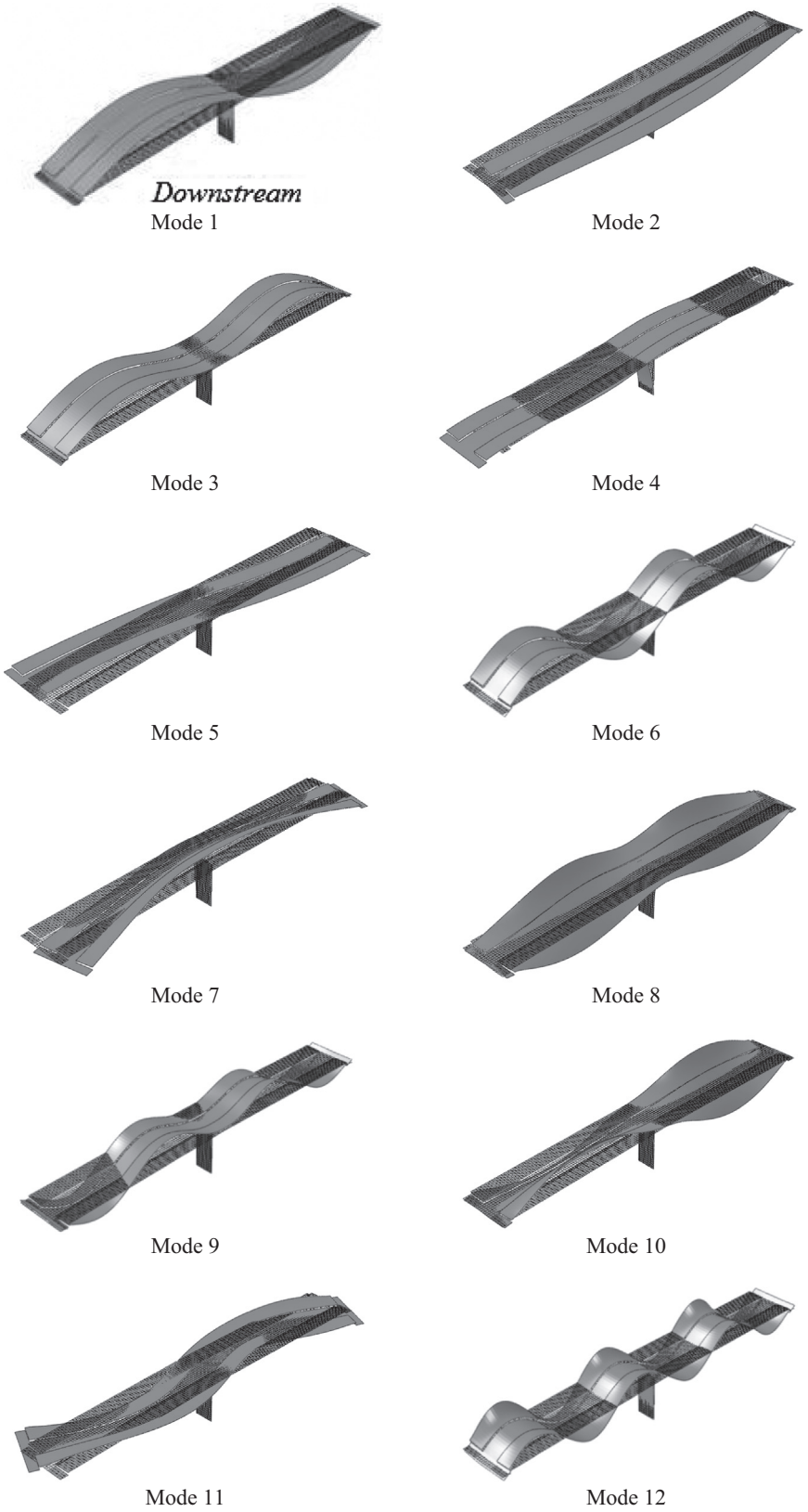

Fig. 7. Numerical modal shapes for the first 12 vibration modes obtained from the first identification problem (ABAQUS).

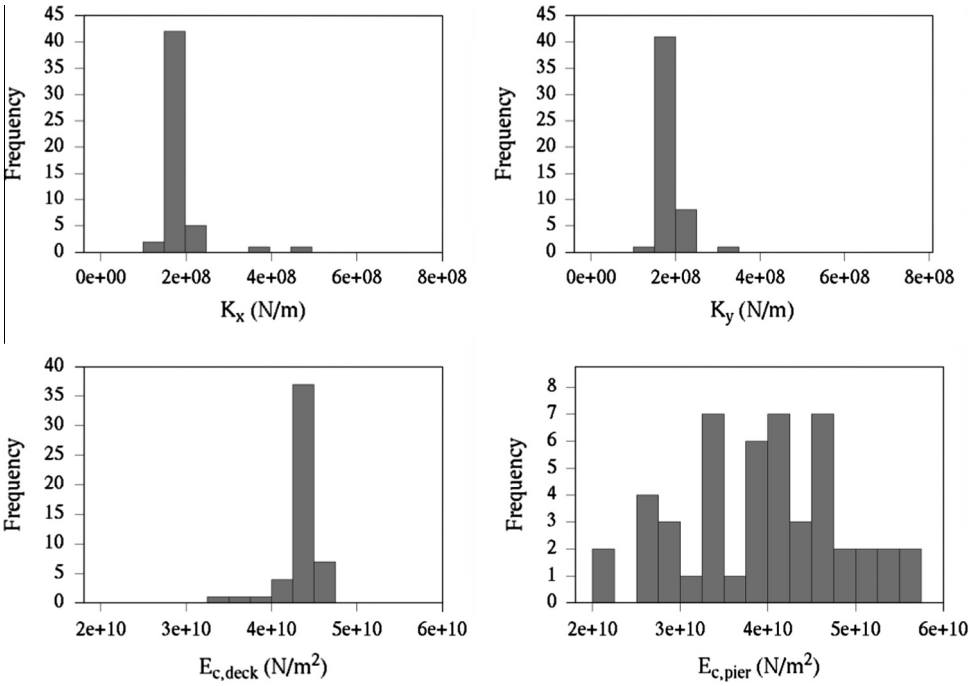

Fig. 8. Distribution of sought parameters in the population at generation 21 (Analysis D1).

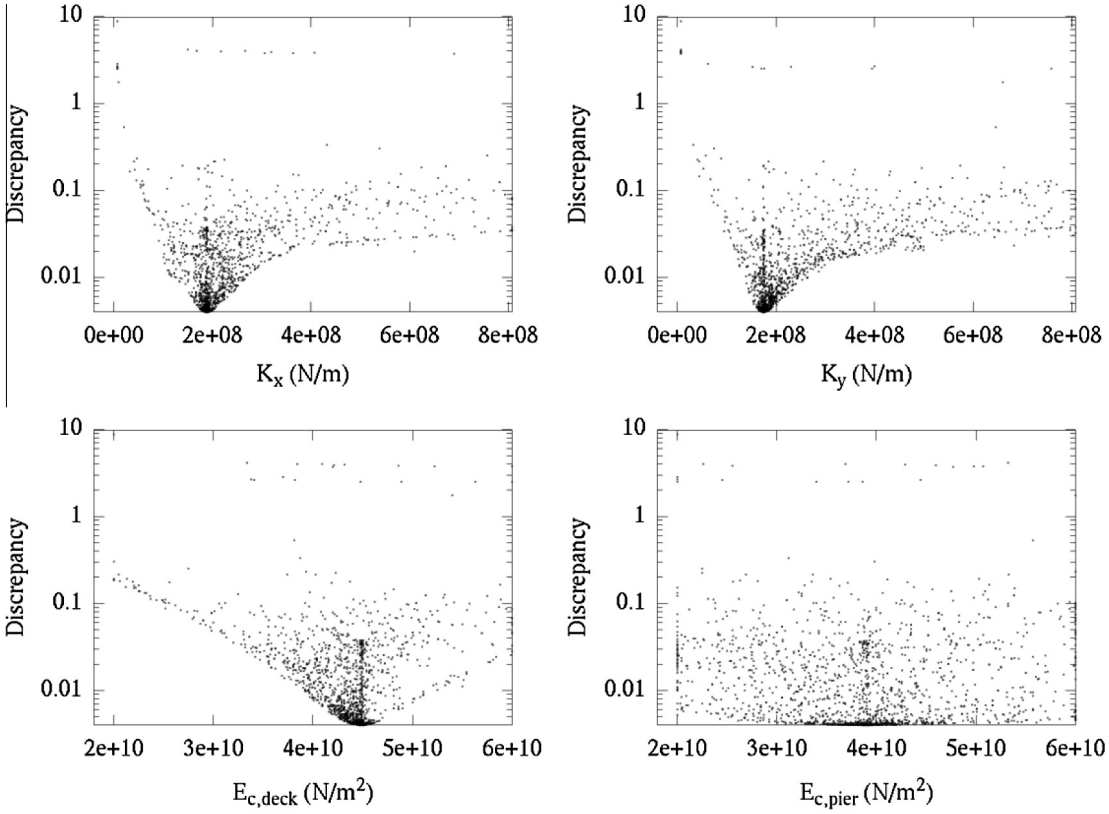

Fig. 9. Parameter–discrepancy plots for dynamic analysis D1.

1. For the analysed individual the MAC matrix is evaluated as in Table 5.
2. For the ith row (experimental mode), the kth computed mode such that $MAC_{ik} = \max_j MAC_{ij}$ $(j = 1,\ldots,N_M)$ is identified.
3. If the $MAC_{ik} \geqslant 50\%$ (minimum consistency) and $i \neq k$ (switch), the ith and kth computed fundamental periods are exchanged.
4. Two discrepancy terms are then evaluated as (see Appendix A):

$$\omega_{2,T}(\boldsymbol{p}) = \sum_{i=1}^{N_M} \frac{f_{ref}}{\Delta f_i}\left(\frac{T_{i,comp}(\boldsymbol{p}) - T_{i,exp}}{T_{exp,max}}\right)^2$$
$$\omega_{2,MAC}(\boldsymbol{p}) = \sum_{i=1}^{N_M} \frac{T_{i,exp}}{T_{exp,max}}\left(1 - \max_j(MAC_{ij}(\boldsymbol{p}))\right)^2 \quad (4)$$

Table 6
Analyses with different objective weights for building Pareto Front in analysis D2.

Analysis	$w_{2,T}$	$w_{2,MAC}$
D2a	1	0
D2b	1	1
D2c	1	10
D2d	1	100
D2e	1	500
D2f	1	1000
D2g	0	1

where $f_{ref} = 1$ Hz is the normalising factor; Δf_i is the uncertainty for ith frequency and $N_M, T_{i,comp}(\boldsymbol{p}), T_{i,exp}, T_{exp,max}, MAC_{ij}(\boldsymbol{p})$ are described in Section 4.3.2.

$\omega_{2,T}$ and $\omega_{2,MAC}$ respectively measure the period and the modal shape discrepancy: the single-objective optimisation problem has thus been replaced by a multi-objective problem. In general, the solution of a multi-objective optimisation problem is represented by a set of nondominated alternatives, called Pareto Front [36], for which none of the objective functions can be improved in value without degrading some of the other objectives. Most methods for solving a multi-objective optimisation problem, such as the Weighted Sum Method (WSM), convert it into a simpler problem, in which a scalar function of the objectives is minimised or maximised. The WSM transforms multiple objectives into an aggregated scalar objective function by multiplying each objective function ω_i by a weighting factor w_i and then summing up all the contributions. If all weighting factors are positive, then it is guaranteed that the solution of the scalar problem belongs to the Pareto Front of the original multi-objective problem [37].

In the problem described in this section, no prior evidence suggests which weights are best suited. For this reason, it is interesting to track the whole Pareto Front, allowing the Decision Maker to choose the best solution a posteriori. This was achieved by performing different optimisation analyses with different weights $w_{2,T}$ and $w_{2,MAC}$, multiplying respectively $\omega_{2,T}$ and $\omega_{2,MAC}$ (Table 6).

The individuals processed in all analyses and the Pareto Front are shown in Fig. 10a and b, where the solutions of the (single-objective) optimisation problems involving only $\omega_{2,T}$ (analysis D2a) and $\omega_{2,MAC}$ (analysis D2g) are also highlighted. It is possible to notice that while, when varying the input parameters $\boldsymbol{p}$, the period discrepancy term $\omega_{2,T}$ changes its value by several orders of magnitude, the variation range of $\omega_{2,MAC}$ is much more limited, being comprised between 0.22 and 1.0. The Pareto Front (represented in Fig. 10b with limited x-range for a better visualisation) clearly shows that the solution of analysis D2g (minimisation of the modal shape discrepancy) implies a very high $\omega_{2,T}$ value, close to the maximum in its range. On the contrary, the minimisation of the period term $\omega_{2,T}$ (analysis D2a) only involves a slight increment in $\omega_{2,MAC}$ compared to the minimum. In other words, the best solution in terms of modal shape is not acceptable as far as the period discrepancy is concerned; the best solution in terms of period is near-optimal even for the modal shape.

For this reason, the point identified as "Optimal $\omega_{2,T}$" in Fig. 10b can be chosen as the solution of the identification problem D2. Its properties are shown in Table 7. It must be noted that the values slightly diverge from the solution reported in Table 3 (in particular K_y increased by less than 5%) for analysis D1 because, in constructing the discrepancy function, the periods are now coupled based on the modal shape consistency, whereas in D1 they were sequentially paired. The differences are nevertheless negligible.

The closeness between K_x and K_y values confirms that the isolator may be considered isotropic in the two horizontal directions, as can also be assumed for constructive reasons. Being the values reported in Table 7 only slightly different from those shown in Table 3, the comparisons between experimental and computed periods and MACs are not reported for the sake of brevity. The

Table 7
Solution of the dynamic identification problem D2.

Parameter	Value
K_x (MN/m)	186.9
K_y (MN/m)	181.5
$E_{c,pier}$ (GPa)	38.8
$E_{c,deck}$ (GPa)	44.7

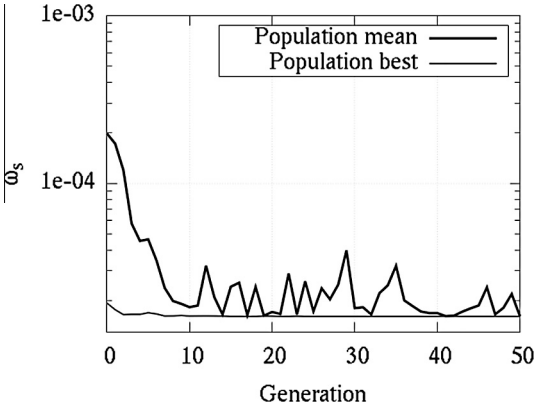

Fig. 11. Static identification analysis S.

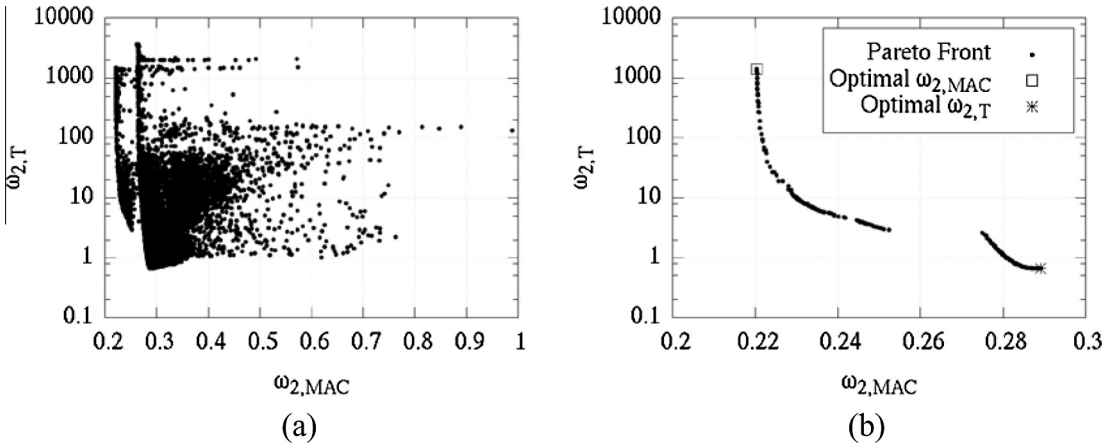

Fig. 10. Multi-objective optimisation D2: (a) all individuals processed, and (b) Pareto Front.

solution still presents some modes which are not consistent with the experimental data (mode pairs 6–8, 7–6, 8–10), and the application of the rule pairing modes according to the modal shape in the discrepancy function does not resolve the switch. Although the approach based on periods and modal shapes in principle allows one to account for a number of factors (uncertainty of measures, influence of lower modes, mode pairing, modal shapes), the results are very close to the ones obtained using a simpler discrepancy function based on sequentially paired periods. Whereas in this specific case the first approach can be used without notable loss of accuracy, nothing can be inferred in general, and since the second approach is more powerful, it is recommended for different situations.

4.3.4. Static identification (S)

Compared to the dynamic analyses, static identification is less complex in the definition of the objective to be minimised. As described in Section 4.3, two loading conditions were considered, and the vertical displacements were recorded respectively in 17 and in 10 points (Fig. 5). The discrepancy function to be minimised is:

$$\omega_s(\boldsymbol{p}) = \sum_{i=1}^{N_L}\sum_{j=1}^{N_{P,i}}\left(u_{j,i,comp}(\boldsymbol{p}) - u_{j,i,exp}\right)^2 \tag{5}$$

where $N_L = 2$ is the number of the load conditions, $N_{P,i}$ is the number of measurements for the ith loading condition, $u_{j,i,exp}$ and $u_{j,i,comp}$ are respectively the experimental and the computed displacements at point j in loading condition i. The results in terms of population mean and best individual are shown in Fig. 11.

It may be seen from the parameter–discrepancy plots (Fig. 12) that the discrepancy is minimally affected by the isolator stiffnesses and the pier concrete Young modulus, and so they should be considered as not identifiable by means of the studied static tests. The discrepancy function can basically be considered as a function of $E_{c,deck}$ only, and its minimum is attained at

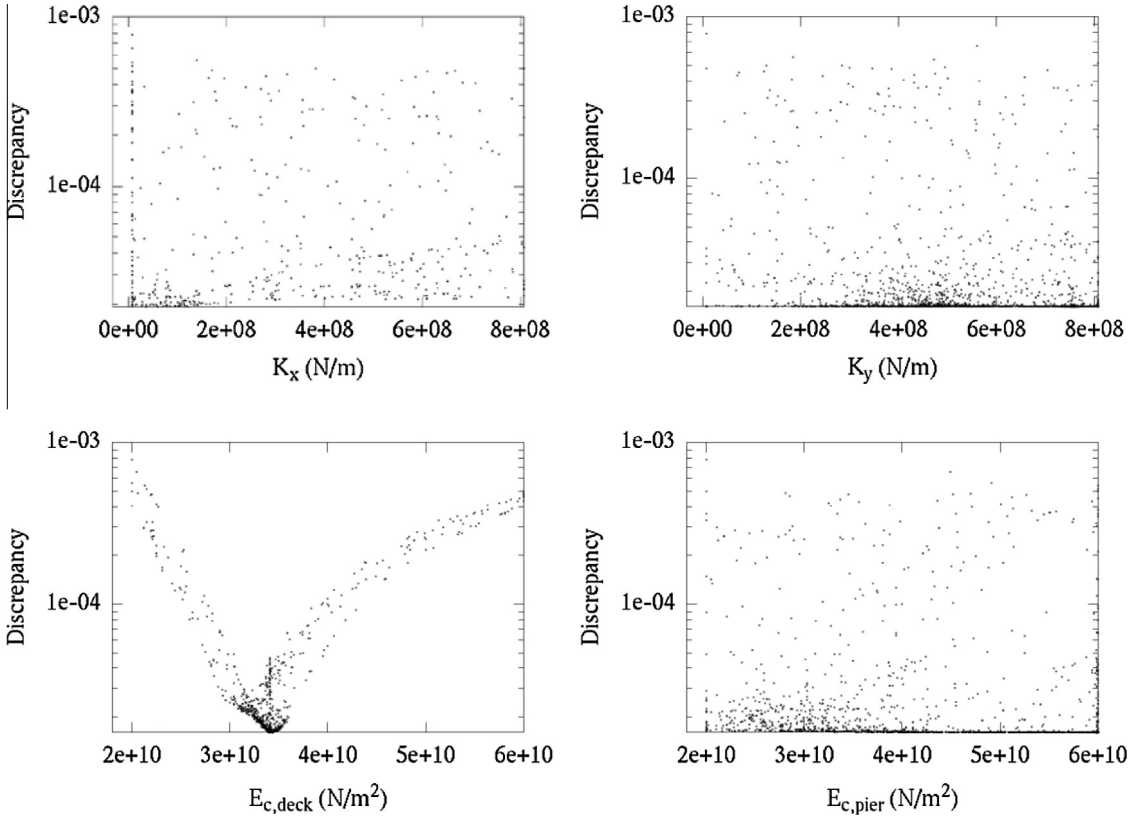

Fig. 12. Parameter–discrepancy plots for static identification analysis S.

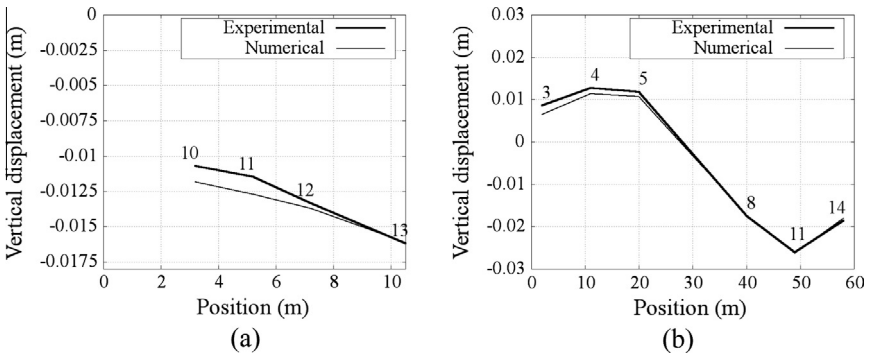

Fig. 13. Comparison between measured and computed displacements (a) in the transverse cross-section in load condition 1 and (b) along the bridge axis in load condition 2. The sensor numbers correspond to the ones displayed in Fig. 5.

$E_{c,deck} = 34.1$ MPa. A comparison between measured and computed vertical displacements in the deck for two load conditions is displayed in Fig. 13.

According to Model Code 2010 [38], the concrete Young modulus E_{ci} at 28 days can be estimated from the specified characteristic strength f_{ck}:

$$E_{ci} = E_{c0} \cdot \alpha_E \cdot \left(\frac{f_{ck} + \Delta f}{10}\right)^{1/3} \tag{6}$$

where $E_{c0} = 21.5 \cdot 10^3$ MPa; $\alpha_E = 1.0$ for quartzite aggregates and $\Delta f = 8$ MPa.

For the C35/45 concrete utilised for the deck, in absence of further information, using Eq. (6), we obtain $E_{ci} = 34.96$ MPa which is in good agreement with the solution of the identification analysis. On the contrary, the solution of the dynamic identification problems D1 (Table 3) reads $E_{c,deck} = 44.9$ MPa. In [39] it has been reported that ratio E_{dyn}/E_{static} (where E_{dyn} and E_{static} are respectively the dynamic and the static concrete Young modulus) is generally included in the range 1.2–1.4 depending on the concrete strength. This is confirmed in the analysed case, where $\frac{E_{dyn}}{E_{static}} = 1.29$.

5. Conclusions

In this work, an inverse approach based on GA was applied for the identification of the main material properties of a base-isolated bridge, based on past static and dynamic test measurements reported in the literature. The identification process took into account both types of experimental data, and as far as dynamic data are concerned, different possibilities were considered for the discrepancy function to be minimised, accounting for several factors (importance of lower modes, accuracy of period estimation, etc.). The use of Genetic Algorithms proved successful, and a critical approach to the solution provided gave an interesting insight on the sensitivity of the solution on the sought parameters. In particular:

- The study of the parameter distribution when convergence is achieved and the parameter–discrepancy plot, clearly show which parameter affects more the discrepancy function and thus may be considered correctly estimated (namely deck Young modulus for both types of tests, and isolator stiffnesses for dynamic identification only).
- Some well-known effects, such as the high stiffness of isolators for small displacements and the ratio between dynamic and static concrete Young modulus were correctly highlighted by the analyses. Although in the current work some further possible influencing parameters have been fully neglected (e.g. friction phenomena or possible contribution of expansion joints), findings obtained for the elastomeric isolators resulted in close agreement with other literature research studies.
- The importance of modal shapes as far as the dynamic identification process is concerned is negligible with respect to the period discrepancy. However, if it is not the case it is possible to consider two objectives to minimise, namely period discrepancy and modal shape consistency and track the Pareto Front of the multi-objective optimisation problem.
- It is not possible to assess isolator stiffnesses by means of static tests.

The generality of the proposed approach makes it suitable for a wide range of material estimation, given that a detailed mathematical or numerical model is available. Further research will exploit the possibilities offered by the method for different structures and materials.

Appendix A

Let i be the mode under consideration. The period discrepancy between the numerical model and the experimental outcome is:

$$\left(\frac{T_{i,comp}(\boldsymbol{p}) - T_{i,exp}}{T_{exp,max}}\right)^2 \tag{A.1}$$

The experimental data consider different uncertainties for the modal frequencies Δf_i: they are described in the third column of Table 1, where the ith fundamental frequency is reported as $f_i \pm \Delta f_i$. Since we want to give smaller weight to more uncertain modes (greater Δf_i), the term (1) is multiplied by the weight $\frac{f_{ref}}{\Delta f_i}$, where $f_{ref} = 1$ Hz is a normalising factor needed to make the weight dimensionless. Summing up the contributions of N_M modes, the period term to minimise is thus:

$$\omega_{2,T}(\boldsymbol{p}) = \sum_{i=1}^{N_M} \frac{f_{ref}}{\Delta f_i} \left(\frac{T_{i,comp}(\boldsymbol{p}) - T_{i,exp}}{T_{exp,max}}\right)^2 \tag{A.2}$$

Let us consider modal shapes now. $\max_j(MAC_{ij}(\boldsymbol{p}))$ is the maximum MAC coefficient between the experimental mode i and the numerical modes and thus identifies the best match among modal shapes. Perfect consistency implies $\max_j(MAC_{ij}(\boldsymbol{p})) = 1$, so the term to insert in the discrepancy function is:

$$(1 - \max_j(MAC_{ij}(\boldsymbol{p})))^2 \tag{A.3}$$

In order to give larger weight to the lowest modes (largest periods), this term is multiplied by the factor $\frac{T_{i,exp}}{T_{exp,max}}$, where the denominator $T_{exp,max}$ acts as a normalising constant.

Summing up the contribution of N_M modes the second objective to minimise is:

$$\omega_{2,MAC}(\boldsymbol{p}) = \sum_{i=1}^{N_M} \frac{T_{i,exp}}{T_{exp,max}} (1 - \max_j(MAC_{ij}(\boldsymbol{p})))^2 \tag{A.4}$$

References

[1] Chaudhary MTA, Abe M, Fujino Y. Investigation of atypical seismic response of a base-isolated bridge. Eng Struct 2002;24:945–53.
[2] Boroschek RL, Moroni MO, Sarrazin M. Dynamic characteristics of a long span seismic isolated bridge. Eng Struct 2003;25:1479–90.
[3] Sarrazin M, Moroni O, Roesset JM. Evaluation of dynamic response characteristics of seismically isolated bridges in Chile. Earthq Eng Struct Dyn 2005;34:425–48.
[4] Altunisik AC, Bayraktar A, Sevim B, Ates S. Ambient vibration based seismic evaluation of isolated Gülburnu highway bridge. Soil Dyn Earthq Eng 2011;31:1496–510.
[5] Chaudhary MTA, Abe M, Fujino Y, Yoshida J. System identification of two base-isolated bridges using seismic records. J Struct Eng ASCE 2000;126(10):1187–95.
[6] FIP Industriale SpA, <http://www.fipindustriale.it/>.
[7] Chaudhary MTA, Abe M, Fujino Y. Role of structural details in altering the expected seismic response of base-isolated bridges. Mech Syst Signal Process 2002;16(2):413–28.
[8] Farrar CR, James III GH. System identification from ambient vibration measurements on a bridge. J Sound Vibr 1997;205(1):1–18.
[9] De Sortis A, Antonacci E, Vestroni F. Dynamic identification of a masonry building using forced vibration tests. Eng Struct 2005;27(2):155–65.
[10] Boscato G, Russo S. Free vibrations of pultruded FRP elements: mechanical characterization, analysis, and applications. J Compos Constr 2009;13(6):565–74.
[11] Cunha A, Caetano E. Experimental modal analysis of civil engineering structures. Sound Vib 2006;6(40):12–20.
[12] Van Overschee P, De Moor BLR. Subspace identification for linear systems: theory, implementation, applications, vol. 3. Dordrecht: Kluwer academic publishers; 1996.
[13] Fritzen C-P, Jennewein D, Kiefer T. Damage detection based on model updating methods. Mech Syst Signal Process 1998;12(1):163–85.
[14] Lee CR, Kam TY. System identification of partially restrained composite plates using measured natural frequencies. J Eng Mech 2006;132(8):841–50.
[15] Sanayei M, Imbaro GR, McClain JAS, Brown LC. Structural model updating using experimental static measurements. J Struct Eng 1997;123(6):792–8.

[16] Avril S, Bonnet M, Bretelle A-S, Grediac M, Hild F, Ienny P, Latourte F, Lemosse D, Pagano S, Pagnacco E, Pierron F. Overview of identification methods of mechanical parameters based on full-field measurements. Exp Mech 2008;48(4):381–402.
[17] Bedon C, Morassi A. Dynamic testing and parameter identification of a base-isolated bridge. Eng Struct 2014;60:85–99.
[18] Wolpert DH, Macready WG. No free lunch theorems for optimization. IEEE Trans Evol Comput 1997;1:67–82.
[19] Box MJ, Davies D, Swann WH. Non-linear optimisation techniques. Oliver & Boyd; 1969.
[20] Byrd RH, Schnabel RB, Schultz GA. A trust region algorithm for nonlinearly constrained optimization. SIAM J Numer Anal 1987;24:1152–70.
[21] Goldberg DE. Genetic algorithms in search, optimization and machine learning. Addison-Wesley; 1989.
[22] Trinh TN, Koh CG. An improved substructural identification strategy for large structural systems. Struct Control Health Monitor 2012;19(8):686–700.
[23] Marano GC, Quaranta G, Monti G. Modified genetic algorithm for the dynamic identification of structural systems using incomplete measurements. Comput-Aided Civil Infrastruct Eng 2011;26(2):92–110.
[24] Monti G, Quaranta G, Marano GC. Genetic-algorithm-based strategies for dynamic identification of nonlinear systems with noise-corrupted response. J Comput Civil Eng 2009;24(2):173–87.
[25] Koh C, Perry MJ. Genetic algorithms in structural identification and damage detection. Intelligent computational paradigms in earthquake engineering; 2007. p. 316.
[26] Someya H. Theoretical analysis of phenotypic diversity in real-valued evolutionary algorithms with more-than-one-element replacement. IEEE Trans Evol Comput 2011;15(2):248–66.
[27] Antonov A, Saleev VM. An economic method of computing LP tau-sequence. USSR Comput Math Math Phys 1979;19(1):252–6.
[28] Eshelman LJ, Schaffer JD. Real-coded genetic algorithms and interval-schemata. Foundations of Genetic Algorithms 2. San Mateo: Morgan Kaufman Publishers; 1993. p. 187–202.
[29] Srinivas M, Patnaik LM. Genetic algorithms: a survey. Computer 1994;27(6):17–26.
[30] Chisari C. Inverse techniques for model identification of masonry structures. PhD. Thesis. University of Trieste; 2015.
[31] Chisari C, Macorini L, Amadio C, Izzuddin BA. An inverse analysis procedure for material parameter identification of mortar joints in unreinforced masonry. Comput Struct 2015;155:97–105.
[32] Alessandrini F, Fedrigo D, Coccolo A. The new bridge seismically isolated over the River Fella in Dogna: design validation as a result of structural dynamic tests [in Italian]. Ingegneria Sismica 2009;XXV I(4):41–52.
[33] NTC2008. Norme tecniche per le costruzioni – D.M. 14 Gennaio 2008 [in Italian].
[34] Simulia. ABAQUS v. 6.12 computer software.
[35] Allemang RJ. The modal assurance criterion – twenty years of use and abuse. Sound Vibr 2003;37(8):14–21.
[36] Miettinen K. Nonlinear multiobjective optimization. Springer; 1999. ISBN 978-0-7923-8278-2.
[37] Goicoechea A, Hansen DR, Duckstein L. Multiobjective decision analysis with engineering and business applications. New York, US: John Wiley & Sons; 1982.
[38] Model Code 2010 – Final draft. fib 65. International Federation for Structural Concrete (fib), vol. 1; 2012.
[39] Nagy A. Determination of E-modulus of young concrete with nondestructive method. J Mater Civil Eng 1997;9(1):15–20.